Advances in Difference Equations
a SpringerOpen Journal

RESEARCH Open Access

A priori and a posteriori estimates of the stabilized finite element methods for the incompressible flow with slip boundary conditions arising in arteriosclerosis

Jian Li[1], Haibiao Zheng[2] and Qingsong Zou[3*]

*Correspondence:
mcszqs@mail.sysu.edu.cn
[3]School of Data and Computational Science and Guangdong Province Key Laboratory of Computational Science, Sun Yat-sen University, Guangzhou, China
Full list of author information is available at the end of the article

Abstract

In this paper, we develop the lower order stabilized finite element methods for the incompressible flow with the slip boundary conditions of friction type whose weak solution satisfies a variational inequality. The H^1-norm for the velocity and the L^2-norm for the pressure decrease with optimal convergence order. The reliable and efficient a posteriori error estimates are also derived. Finally, numerical experiments are presented to validate the theoretical results.

MSC: 35L70; 65N30; 76D06

Keywords: Stokes equations; Slip boundary condition; Variational inequality; Finite element methods; A priori error estimates; A posteriori error estimates; Numerical experiments

1 Introduction

Incompressible viscous flow phenomena arise in numerous disciplines in science and engineering. The simplest viscous flow problems involve just one fluid in the laminar regime. Numerical methods for this model have been intensively studied during the past several decades [3, 9, 17, 45]. A critical problem in the construction of numerical methods is to establish the so-called Babuška–Brezzi stability condition. It is known that if the finite element spaces for the velocity and pressure are of the lowest equal-order or lowest order pairs, the corresponding finite element schemes do not satisfy the Babuška–Brezzi condition. For lower order schemes, some stabilized finite element methods are studied and developed in [7, 8, 10, 11, 14, 19, 32, 33, 44]. This numerical instability can be remedied by adding a so-called pressure projection term; see [7, 8, 11, 32].

In this paper, we are interested in the model of the Stokes problem with the slip boundary conditions of friction type [4, 6, 16, 24, 27, 39–42]. This frictional boundary conditions appear in modeling of blood flow in vein of an arterial sclerosis patient and in that avalanche of water and rocks. This model has drawn many experts' attention in the past several decades. However, even now, there are many difficulties arising from this model remain unsolved including a priori and posteriori estimates.

In this paper, we discretize the corresponding variational inequality with the stabilized finite element methods proposed in [8, 28–33, 36, 38]. Since the discrete bilinear form is stable, our discrete variational inequality admits a unique finite element solution. An important contribution of the paper is to analyze the a priori estimates for the finite element solutions. The optimal result is first valid for both the unstable linear–constant and the linear–linear pairs. Another important contribution is the a posteriori estimates. Although a posteriori estimates have been intensively studied for the Stokes problems with Dirichlet boundary conditions [2, 5, 26, 31, 46–48], the corresponding result for the Stokes problems with nonlinear slip boundary conditions has not been completely solved. Here, we obtain the error estimators constitutes of the standard error indicators for the Stokes problem with Dirichlet boundary condition and error indicators on the slip boundary. With a rigorous proof, we show that the error estimators are reliable. The efficiency of the standard error indicators is also discussed. Numerical experiments show that the error indicators on the slip boundary are also efficient, its complete theoretical proof is still to be derived.

The paper is organized as follows. In Sect. 2, we introduce a Stokes problem with a slip boundary and the stabilized finite element methods for this problem. The optimal a priori error estimate is given in Sect. 3. While in Sect. 4, the a posteriori error estimate is provided. In the final section, numerical experiments are performed to validate our theory developed in previous sections.

Throughout this paper, "$A \lesssim B$" means that A can be bounded by B multiplied with a generic constant depending only on the shape regularity of the underlying grid or the given domain, "$A \simeq B$" stands for "$A \lesssim B$" and "$B \lesssim A$". In addition, the spaces of consisting of vector-valued and scalar-valued functions will be denoted in bold face and usual face, respectively.

2 The Stokes problem with slip boundary conditions and its finite element solution

We consider the following Stokes equations with the slip boundary conditions of friction type:

$$-\mu\Delta\mathbf{u} + \nabla p = \mathbf{f}, \qquad \operatorname{div}\mathbf{u} = 0, \quad \text{in } \Omega, \tag{2.1}$$

$$\mathbf{u} = 0, \quad \text{on } \Gamma_D, \tag{2.2}$$

$$\mathbf{u}_n = 0, \qquad |\sigma_\tau| \le g, \qquad \sigma_\tau\mathbf{u}_\tau + g|\mathbf{u}_\tau| = 0, \quad \text{on } \Gamma. \tag{2.3}$$

Here Ω is a bounded convex polygon of R^2, its boundary $\partial\Omega$ is flat and includes two connected portions Γ_D and Γ. The portions Γ and Γ_D are not empty. The functions $\mathbf{u}(x)$, $p(x)$ and $\mathbf{f}(x)$ represent the velocity vector, the pressure, and the prescribed body force, respectively; the coefficient $\mu > 0$ stands for the viscosity and g is a given positive scalar function. Here and in what follows, the unit outward normal to the boundary is denoted by $\mathbf{n}$ and for a vector $\mathbf{v}$ defined on the boundary, we use $\mathbf{v}_n = \mathbf{v}\cdot\mathbf{n}$ and $\mathbf{v}_\tau = \mathbf{v} - \mathbf{v}_n\mathbf{n}$ to denote the normal and tangential component of $\mathbf{v}$, respectively. The function $\sigma_\tau = \mu\frac{\partial\mathbf{u}_\tau}{\partial n}$ denotes tangential component of stress vector defined on Γ.

In the following, we present the weak formulation of (2.1)–(2.3). Let $H^m(\Omega)$ be the Sobolev space with the norm $\|\cdot\|_{m,\Omega}$. Note that in the case $m = 0$, we set $H^0(\Omega) = L^2(\Omega)$.

Let $H_0^1(\Omega)$ be the subspace of functions in $H^1(\Omega)$ with zero trace on $\partial\Omega$. We define the following spaces [1]:

$$\mathbf{V} = \left\{\mathbf{v} \in \left[H^1(\Omega)\right]^2 : \mathbf{v}|_{\Gamma_D} = 0, \mathbf{v}_n|_\Gamma = 0\right\},$$
$$Q = L_0^2(\Omega) \equiv \left\{q \in L^2(\Omega) : \int_\Omega q\, d\mathbf{x} = 0\right\}.$$

We denote the inner product and norm on Ω and its boundary Γ, respectively, by

$$(\mathbf{u}, \mathbf{v})_\Omega = \int_\Omega \mathbf{u} \cdot \mathbf{v}\, d\mathbf{x}, \qquad \langle \mathbf{u}, \mathbf{v}\rangle_\Gamma = \int_\Gamma \mathbf{u} \cdot \mathbf{v}\, ds,$$
$$\|\mathbf{u}\|_{0,\Omega} = (\mathbf{u}, \mathbf{u})^{1/2}, \qquad \|\mathbf{u}\|_{0,\Gamma} = \langle \mathbf{u}, \mathbf{u}\rangle_\Gamma.$$

We introduce a norm $|||\cdot|||$ in the coupled space $\mathbf{V} \times Q$ by

$$\left|\left|\left|(\mathbf{v}, q)\right|\right|\right| = \left(\mu\|\nabla\mathbf{v}\|_0^2 + \|q\|_0^2\right)^{1/2}, \quad \forall (\mathbf{v}, q) \in \mathbf{V} \times Q,$$

where

$$\|\nabla\mathbf{v}\|_0 = (\nabla\mathbf{v}, \nabla\mathbf{v})^{1/2}, \quad \forall \mathbf{v} \in \mathbf{V},$$

and

$$\|p\|_0 = (p, p)^{1/2}, \quad p \in Q.$$

We define

$$a(\mathbf{u}, \mathbf{v}) = 2\mu\left(\mathbb{D}(\mathbf{u}), \mathbb{D}(\mathbf{v})\right) = \mu(\nabla\mathbf{u}, \nabla\mathbf{v}), \quad \forall \mathbf{u}, \mathbf{v} \in \mathbf{V},$$
$$d(\mathbf{v}, p) = (\operatorname{div}\mathbf{v}, p), \quad (\mathbf{v}, p) \in \mathbf{V} \times Q,$$

where

$$\mathbb{D}(\mathbf{v}) = \frac{1}{2}\left(\nabla\mathbf{v} + \nabla\mathbf{v}^T\right)$$

represents the rate of deformation tensor. Let the bilinear form

$$B\left((\mathbf{u}, p); (\mathbf{v}, q)\right) = a(\mathbf{u}, \mathbf{v}) - d(\mathbf{v}, p) + d(\mathbf{u}, q), \quad \forall (\mathbf{u}, p), (\mathbf{v}, q) \in \mathbf{V} \times Q.$$

Since the bilinear forms $a(\cdot,\cdot)$ and $d(\cdot,\cdot)$ are continuous, the bilinear form $B(\cdot,\cdot)$ is also continuous satisfying

$$B\left((\mathbf{u}, p); (\mathbf{v}, q)\right) \lesssim \left|\left|\left|(\mathbf{u}, p)\right|\right|\right| \left|\left|\left|(\mathbf{v}, q)\right|\right|\right|, \quad \forall (\mathbf{u}, p), (\mathbf{v}, q) \in \mathbf{V} \times Q. \tag{2.4}$$

Moreover, we have the following inf-sup property:

$$\left|\left|\left|(\mathbf{u}, p)\right|\right|\right| \lesssim \sup_{(\mathbf{v}, q) \in (\mathbf{V}, Q)} \frac{|B((\mathbf{u}, p); (\mathbf{v}, q))|}{|||(\mathbf{v}, q)|||}. \tag{2.5}$$

Here, the hidden constant is independent of $(\mathbf{u}, p)$ and $(\mathbf{v}, q)$.

Now we introduce the barrier term against slip on Γ as

$$j(z) = \int_{\Gamma} g|z|\,ds, \quad z \in L^2(\Gamma).$$

Obviously, j is a continuous functional defined on $L^2(\Gamma)$.

The weak formulation of the Stokes equations (2.1)–(2.3) reads (cf. [16])

Find $(\mathbf{u}, p) \in \mathbf{V} \times Q$ such that

$$B\big((\mathbf{u},\mathbf{p});(\mathbf{v}-\mathbf{u},q)\big) + j(\mathbf{v}_\tau) - j(\mathbf{u}_\tau) \geq (f, \mathbf{v}-\mathbf{u}), \quad \forall (\mathbf{v}, q) \in \mathbf{V} \times Q. \tag{2.6}$$

Also from [16], we know that (2.6) admits a unique solution. Moreover, if $\Gamma_D \in C^2$, $\Gamma \in C^4$, $\mathbf{f} \in [L^2(\Omega)]^2$ and $g \in H^1(\Gamma)$, then the solution $(\mathbf{u}, p) \in [H^2(\Omega)]^2 \times H^1(\Omega)$ (cf. [42]).

We next present the stabilized finite element methods for the present model. The stabilized finite element methods have been introduced in [8, 11, 32] for the Stokes equations with Dirichlet boundary conditions.

Let $\mathcal{T}_h$ be a regular, quasi-uniform triangulation of the polygonal domain Ω into a union of triangles [12, 13]. Associated with $\mathcal{T}_h = \{K\}$, we consider the finite element spaces for the velocity and pressure: $V_h \subset V$ and $Q_h \subset Q$ with $h = \max\{h_K : K \in \mathcal{T}_h\}$.

We first define

$$\mathbf{V}_h = \big\{\mathbf{v} \in \mathbf{V} : \mathbf{v}|_K \in \big[P_1(K)\big]^2, \forall K \in \mathcal{T}_h\big\},$$

$$Q_h = \begin{cases} Q_h^0 \equiv \{q \in Q : q|_K \in P_0(K), \forall K \in \mathcal{T}_h\}, \\ Q_h^1 \equiv \{q \in Q : q|_K \in P_1(K), \forall K \in \mathcal{T}_h\}, \end{cases}$$

where P_1 and P_0 denote the spaces of polynomials of degree 1 or 0 on set K, respectively. It is well known that, for all $(\mathbf{v}, q) \in [W^{2,\infty}(\Omega)]^2 \times H^1(\Omega)$, we have the approximation properties:

$$\inf_{(\mathbf{v}_h, q_h) \in \mathbf{V}_h \times Q_h} |||(\mathbf{v}-\mathbf{v}_h, q-q_h)||| \lesssim h\big(\|\mathbf{v}\|_2 + \|q\|_1\big), \tag{2.7}$$

$$\inf_{\mathbf{v}_h \in \mathbf{V}_h} \|\mathbf{v}-\mathbf{v}_h\|_{0,\Gamma} \lesssim h^2 \|\mathbf{v}\|_{2,\infty}. \tag{2.8}$$

Here, we aim to formulate the stabilized mixed finite element methods for the lowest equal-order pair $\mathbf{V}_h \times Q_h^1$ and for the lowest order pair $\mathbf{V}_h \times Q_h^0$. These two pairs are unstable and do not satisfy the so-called Babuška–Brezzi stability condition. A local pressure projection method is recalled in [8, 11, 32]. Let Π_h be the elementwise L^2-projection

$$\Pi_h = \begin{cases} \Pi_0 : L^2(\Omega) \to Q_h^1, & \text{for } P_1 - P_0, \\ \Pi_1 : L^2(\Omega) \to Q_h^0, & \text{for } P_1 - P_1. \end{cases}$$

Here, the operators Π_0 and Π_1 are, respectively, applied to stabilize the lowest equal-order pair $\mathbf{V}_h \times Q_h^1$ and the lowest order pair $\mathbf{V}_h \times Q_h^0$. Furthermore, the mapping satisfies the following properties [8, 32]:

$$\|\Pi_h p\|_0 \lesssim \|p\|_0, \quad \forall p \in Q_h, \tag{2.9}$$

$$\|p - \Pi_h p\|_0 \lesssim h\|p\|_1, \quad \forall p \in H^1(\Omega) \cap Q_h. \tag{2.10}$$

Now, we are in a position to introduce the stabilized bilinear form (cf. [8, 11, 32])

$$G(p_h, q_h) = (p_h - \Pi_h p_h, q_h - \Pi_h q_h). \tag{2.11}$$

We define the bilinear form for all $(\mathbf{u}_h, p_h), (\mathbf{v}_h, q_h) \in \mathbf{V}_h \times Q_h$ by

$$\mathcal{B}_h\big((\mathbf{u}_h, p_h); (\mathbf{v}_h, q_h)\big) = B\big((\mathbf{u}_h, p_h); (\mathbf{v}_h, q_h)\big) + G(p_h, q_h).$$

The finite element approximation to (2.6) is to find $(\mathbf{u}_h, p_h) \in \mathbf{V}_h \times Q_h$ such that, for all $(\mathbf{v}_h, q_h) \in \mathbf{V}_h \times Q_h$,

$$\mathcal{B}_h\big((\mathbf{u}_h, p_h); (\mathbf{v}_h - \mathbf{u}_h, q_h)\big) + j(\mathbf{v}_{h\tau}) - j(\mathbf{u}_{h\tau}) \geq (\mathbf{f}, \mathbf{v}_h - \mathbf{u}_h). \tag{2.12}$$

By the definition of $\mathcal{B}_h(\cdot, \cdot)$, (2.12) is for all $\mathbf{v}_h \in \mathbf{V}_h$ equivalent to

$$a(\mathbf{u}_h, \mathbf{v}_h - \mathbf{u}_h) - d(\mathbf{v}_h - \mathbf{u}_h, p_h) + j(\mathbf{v}_{h\tau}) - j(\mathbf{u}_{h\tau}) \geq (\mathbf{f}, \mathbf{v}_h - \mathbf{u}_h), \tag{2.13}$$

and for all $q_h \in Q_h$,

$$d(\mathbf{u}_h, q_h) + G(p_h, q_h) = 0. \tag{2.14}$$

3 A priori error estimates

In this section, we estimate the $|||\cdot|||$ norm of the error between the exact solution $(\mathbf{u}, p)$ of (2.6) and the finite element solution $(\mathbf{u}_h, p_h)$ of (2.12).

To this end, we first study the properties of the bilinear form $\mathcal{B}_h(\cdot, \cdot)$. By a similar approach in [8, 32], it is easy to verify the following continuity: for all $(\mathbf{v}_h, q_h)$, $(\mathbf{w}_h, \lambda_h) \in \mathbf{V}_h \times Q_h$,

$$\big|\mathcal{B}_h\big((\mathbf{v}_h, q_h); (\mathbf{w}_h, \lambda_h)\big)\big| \lesssim |||(\mathbf{v}_h, q_h)||| \, |||(\mathbf{w}_h, \lambda_h)|||, \tag{3.1}$$

where the hidden constant is independent of the mesh size h. Moreover, by similar arguments in [20, 25, 33, 39, 40], it is not hard to establish the following inf-sup property: for all $(\mathbf{v}_h, q_h) \in \mathbf{V}_h \times Q_h$,

$$|||(\mathbf{v}_h, q_h)||| \lesssim \sup_{(\mathbf{w}_h, \lambda_h) \in \mathbf{V}_h \times Q_h} \frac{\mathcal{B}_h((\mathbf{v}_h, q_h); (\mathbf{w}_h, \lambda_h))}{|||(\mathbf{w}_h, \lambda_h)|||}. \tag{3.2}$$

Due to (3.1), (3.2) and the fact that $j(\cdot)$ is a continuous functional defined on the convex set $\mathbf{V}_h \times Q_h$, the discrete problem (2.12) has a unique solution [4, 40].

For completeness, we are ready to prove the following theorem for the model approximated by the lower order finite element pairs.

Theorem 3.1 *Let* $(\mathbf{u}, p) \in \mathbf{V} \times Q$ *and* $(\mathbf{u}_h, p_h) \in \mathbf{V}_h \times Q_h$ *be solutions of* (2.6) *and* (2.12), *respectively. If* $(\mathbf{u}, p) \in [H^2(\Omega)]^2 \times H^1(\Omega)$, *then*

$$|||(\mathbf{u} - \mathbf{u}_h, p - p_h)||| \lesssim h\big(\|\mathbf{u}\|_2 + \|p\|_1 + \|\mathbf{u}\|_2^{\frac{1}{2}}\big), \tag{3.3}$$

where the hidden constant only depends on the data $(\mu, \mathbf{f}, g, \Omega)$.

Proof First, we estimate $\|\nabla(\mathbf{u}-\mathbf{u}_h)\|_0$. By the triangle inequality, for all $\mathbf{v}_h \in \mathbf{V}_h$,

$$\big\|\nabla(\mathbf{u}-\mathbf{u}_h)\big\|_0 \le \big\|\nabla(\mathbf{u}-\mathbf{v}_h)\big\|_0 + \big\|\nabla(\mathbf{u}_h-\mathbf{v}_h)\big\|_0.$$

By the definition of the bilinear $\mathcal{B}_h$, for all $(\mathbf{v}_h, q_h) \in \mathbf{V}_h \times Q_h$,

$$\mu\big\|\nabla(\mathbf{u}_h-\mathbf{v}_h)\big\|_0^2 \le \mathcal{B}_h\big((\mathbf{u}_h-\mathbf{v}_h, p_h-q_h), (\mathbf{u}_h-\mathbf{v}_h, p_h-q_h)\big) = I_1 - I_2, \tag{3.4}$$

where

$$I_1 = \mathcal{B}_h\big((\mathbf{u}_h, p_h), (\mathbf{u}_h-\mathbf{v}_h, p_h-q_h)\big)$$

and

$$I_2 = \mathcal{B}_h(\mathbf{v}_h, q_h), (\mathbf{u}_h-\mathbf{v}_h, p_h-q_h)).$$

By (2.12), we have

$$I_1 \le (f, \mathbf{u}_h-\mathbf{v}_h) + j(\mathbf{v}_{h\tau}) - j(\mathbf{u}_{h\tau}). \tag{3.5}$$

Taking $(\mathbf{v}, q) = (\mathbf{u}_h-\mathbf{v}_h+\mathbf{u}, p_h-q_h)$ in (2.6), we have

$$\begin{aligned}(f, \mathbf{u}_h-\mathbf{v}_h) &\le B\big((\mathbf{u}, p), (\mathbf{u}_h-\mathbf{v}_h, p_h-q_h)\big) + j\big((\mathbf{u}_h-\mathbf{v}_h+\mathbf{u})_\tau\big) - j(\mathbf{u}_\tau)\\ &\le \mathcal{B}_h\big((\mathbf{u}, p), (\mathbf{u}_h-\mathbf{v}_h, p_h-q_h)\big) - G(p, p_h-q_h)\\ &\quad + j\big((\mathbf{u}_h-\mathbf{v}_h+\mathbf{u})_\tau\big) - j(\mathbf{u}_\tau).\end{aligned} \tag{3.6}$$

Using the Hölder inequality, it is easy to verify that, for all $\mathbf{v} \in \mathbf{V}$,

$$\begin{aligned}j(\mathbf{v}_{h\tau}) - j(\mathbf{u}_\tau) &= \int_\Gamma g|\mathbf{v}_{h\tau}|\,ds - \int_\Gamma g|\mathbf{u}_\tau|\,ds\\ &\le \int_\Gamma g|\mathbf{v}_{h\tau}-\mathbf{u}_\tau|\,ds\\ &\lesssim h_\Gamma^{1/2}\|g\|_{\infty,\Gamma}\|\mathbf{v}_{h\tau}-\mathbf{u}_\tau\|_{0,\Gamma},\end{aligned} \tag{3.7}$$

where the mesh size h_Γ is the largest scale of the set $K \cap \Gamma$.

Moreover, using the definition of $G(\cdot,\cdot)$ and the Hölder inequality, yields

$$\begin{aligned}G(p, p_h-q_h) &= \big(p-\Pi_h p, (p_h-q_h) - \Pi_h(p_h-q_h)\big)\\ &\le \|p-\Pi_h p\|_0\|p_h-q_h\|_0.\end{aligned} \tag{3.8}$$

Substituting (3.6) and (3.7) into (3.5), we have

$$\begin{aligned}I_1 \le{}& \mathcal{B}_h\big((\mathbf{u}, p), (\mathbf{u}_h-\mathbf{v}_h, p_h-q_h)\big) + 2h_\Gamma^{1/2}\|g\|_{\infty,\Gamma}\|\mathbf{u}_\tau-\mathbf{v}_{h\tau}\|_{0,\Gamma}\\ &+ \|p-\Pi_h p\|_0\|p_h-q_h\|_0.\end{aligned}$$

Therefore,

$$\begin{aligned} I_1 - I_2 &\le \mathcal{B}_h\big((\mathbf{u}-\mathbf{v}_h, p-q_h), (\mathbf{u}_h-\mathbf{v}_h, p_h-q_h)\big) \\ &\quad + \|p-\Pi_h p\|_0 \|p_h-q_h\|_0 + 2h_\Gamma^{1/2}\|g\|_{\infty,\Gamma}\|\mathbf{u}_\tau-\mathbf{v}_{h\tau}\|_{0,\Gamma} \\ &\lesssim |||(\mathbf{u}-\mathbf{v}_h, p-q_h)||| \, |||(\mathbf{u}_h-\mathbf{v}_h, p_h-q_h)||| \\ &\quad + \|p-\Pi_h p\|_0 \|p_h-q_h\|_0 + h_\Gamma^{1/2}\|g\|_{\infty,\Gamma}\|\mathbf{u}_\tau-\mathbf{v}_{h\tau}\|_{0,\Gamma}. \end{aligned}$$

Then, by (3.4) and the Young inequality,

$$\begin{aligned} \|\nabla(\mathbf{u}_h-\mathbf{v}_h)\|_0^2 &\lesssim |||(\mathbf{u}-\mathbf{v}_h, p-q_h)|||^2 + \|p_h-q_h\|_0^2 \\ &\quad + \|p-\Pi_h p\|_0^2 + h_\Gamma^{1/2}\|\mathbf{u}_\tau-\mathbf{v}_{h\tau}\|_{0,\Gamma}. \end{aligned}$$

Consequently

$$\|\nabla(\mathbf{u}-\mathbf{u}_h)\|_0^2 \lesssim |||(\mathbf{u}-\mathbf{v}_h, p-q_h)|||^2 + \|p_h-q_h\|_0^2 + h^2\|p\|_1^2 + h^{1/2}\|\mathbf{u}_\tau-\mathbf{v}_{h\tau}\|_{0,\Gamma}, \tag{3.9}$$

where we have used the fact that $\|p-\Pi_h p\|_0 \lesssim h\|p\|_1$. On the other hand, set that

$$\bar{\mathbf{V}}_h = \big\{\mathbf{v} \in \big[H_0^1(\Omega)\big]^2 : \mathbf{v}|_K \in \big[P_1(K)\big]^2\big\} \subset \mathbf{V}_h.$$

Let $\mathbf{w}_h \in \bar{\mathbf{V}}_h$ and taking $\mathbf{v} = \mathbf{u} \pm \mathbf{w}_h$ separately in (2.6), we obtain

$$a(\mathbf{u}, \mathbf{w}_h) - d(\mathbf{w}_h, p) = (\mathbf{f}, \mathbf{w}_h).$$

Also, taking $\mathbf{v}_h = \mathbf{u}_h \pm \mathbf{w}_h$ separately in (2.12), we obtain

$$a(\mathbf{u}_h, \mathbf{w}_h) - d(\mathbf{w}_h, p_h) = (\mathbf{f}, \mathbf{w}_h).$$

Then, for all $(\mathbf{w}_h, \lambda_h) \in \mathbf{V}_h \times Q_h$, noting that

$$d(\mathbf{u}-\mathbf{u_h}, \lambda_h) + G(p-p_h, \lambda_h) = 0,$$

we can derive from the above two equalities that

$$a(\mathbf{u}-\mathbf{u_h}, \mathbf{w}_h) - d(\mathbf{w}_h, p-p_h) + d(\mathbf{u}-\mathbf{u_h}, \lambda_h) + G(p-p_h, \lambda_h) = 0. \tag{3.10}$$

Then, we can derive the following result from the weak coercivity property in [19]:

$$\begin{aligned} &\|p_h-q_h\|_0 \\ &\lesssim \sup_{(\mathbf{w}_h,\lambda_h)\in(\bar{\mathbf{V}}_h,Q_h)} \frac{\mathcal{B}_h((u_h-v_h, p_h-q_h); (\mathbf{w}_h, \lambda_h))}{|||(\mathbf{w}_h, \lambda_h)|||} \\ &\lesssim \sup_{(\mathbf{w}_h,\lambda_h)\in(\bar{\mathbf{V}}_h,Q_h)} \frac{\mathcal{B}_h((u_h-u, p_h-p); (\mathbf{w}_h, \lambda_h)) + \mathcal{B}_h((u-v_h, p-q_h); (\mathbf{w}_h, \lambda_h))}{|||(\mathbf{w}_h, \lambda_h)|||} \end{aligned}$$

$$\lesssim \left(\sup_{(\mathbf{w}_h,\lambda_h)\in(\bar{\mathbf{V}}_h,Q_h)} \frac{G(p,\lambda_h)}{|||(\mathbf{w}_h,\lambda_h)|||} + \sup_{(\mathbf{w}_h,\lambda_h)\in(\bar{\mathbf{V}}_h,Q_h)} \frac{\mathcal{B}_h((u-v_h,p-q_h);(\mathbf{w}_h,\lambda_h))}{|||(\mathbf{w}_h,\lambda_h)|||} \right)$$

$$\lesssim \big(|||(u-v_h,p-q_h)||| + \|p-\Pi_h p\|_0 \big), \tag{3.11}$$

where the hidden constant only depends on Ω.

Thus, we obtain, for all $(\mathbf{v}_h,q_h)\in\mathbf{V}_h\times Q_h$,

$$|||(\mathbf{u}-\mathbf{u}_h,p-p_h)|||^2 \lesssim |||(\mathbf{u}-\mathbf{v}_h,p-q_h)|||^2 + h^2\|p\|_1^2 + h^{1/2}\|\mathbf{u}_\tau-\mathbf{v}_{h\tau}\|_{0,\Gamma}.$$

Noticing estimates (2.7) and (2.8), the proof of (3.3) is completed. □

4 A posteriori error estimates

In this section, we will derive the a reliable and efficient a posteriori estimates for the error $|||(\mathbf{u}-\mathbf{u}_h,p-p_h)|||$.

Denote by $\mathcal{E}_h$ the set of all of the interior element-edges. For $K\in\mathcal{T}_h$ and $E\in\mathcal{E}_h$, we define the element residual and jump residual by

$$\mathbf{R}_K = \mathbf{f} + \mu\Delta\mathbf{u}_h - \nabla p_h,$$

$$J_E = \left[\frac{\partial\mathbf{u}_h}{\partial\mathbf{n}} - p_h\mathbf{n}\right]_E = [\nabla\mathbf{u}_h - p_h\mathbf{I}]_E\cdot\mathbf{n}.$$

Hereafter, $[q]_E$ denotes the jump of q across an interior side $E\in\mathcal{E}_h$, $\mathbf{n}$ denotes a unit normal of $E\in\mathcal{E}_h$, and $\mathbf{I}$ denotes the identity matrix. We define the elementwise local error indicator for all $K\in\mathcal{T}_h$ by

$$\eta_K^2 = h_K^2\|\mathbf{R}_K\|_{0,K}^2 + \|\operatorname{div}\mathbf{u}_h\|_{0,K}^2 + \sum_{E\in\mathcal{E}_h\cap\partial K} h_E\|J_E\|_{0,E}^2 + \sum_{E\in\Gamma\cap\partial K} h_E^2\|g\|_{\infty,E}^2.$$

Then, the global error estimator can be written by

$$\eta = \left(\sum_{K\in\mathcal{T}_h}\eta_K^2\right)^{1/2}.$$

In the following, we analyze the reliability and efficiency of η. Let $\mathbf{u}_i$ and p_i be the Scott–Zhang interpolation (cf. [43]) of $\mathbf{u}$ and p, respectively. For simplicity, we denote $(\mathbf{e}_i,\epsilon_i) = (\mathbf{u}_i-\mathbf{u}_h,p_i-p_h)$ and $(\mathbf{e},\epsilon) = (\mathbf{u}-\mathbf{u}_h,p-p_h)$.

4.1 Reliability

In this subsection, we show that the error $|||(\mathbf{e},\epsilon)|||$ can be bounded by the estimator η.

Theorem 4.1 *Let $(\mathbf{u},p)\in\mathbf{V}\times Q$ and $(\mathbf{u}_h,p_h)\in\mathbf{V}_h\times Q_h$ be solutions of (2.6) and (2.12), respectively. Then*

$$|||(\mathbf{e},\epsilon)||| \lesssim \eta, \tag{4.1}$$

where the hidden constant is independent of h.

Proof A direct calculation yields

$$B\big((\mathbf{e},\epsilon),(\mathbf{e}_i,\epsilon_i)\big) = B\big((\mathbf{u},p),(\mathbf{e}_i,\epsilon_i)\big) - \mathcal{B}_h\big((\mathbf{u}_h,p_h),(\mathbf{e}_i,\epsilon_i)\big) + G(p_h,\epsilon_i).$$

Then

$$B\big((\mathbf{e},\epsilon),(\mathbf{e}_i,\epsilon_i)\big) = I_1 + I_2,$$

where

$$I_1 = (\mathbf{f},\mathbf{e}_i) - \mathcal{B}_h\big((\mathbf{u}_h,p_h),(\mathbf{e}_i,\epsilon_i)\big) - (\mathbf{f},\mathbf{e}) + B\big((\mathbf{u},p),(\mathbf{e},\epsilon)\big),$$

and

$$I_2 = -(\mathbf{f},\mathbf{e}_i-\mathbf{e}) + B\big((\mathbf{u},p),(\mathbf{e}_i-\mathbf{e},\epsilon_i-\epsilon)\big) + G(p_h,\epsilon_i).$$

Taking $(\mathbf{v}_h,q_h) = (\mathbf{u}_i,p_i-p_h)$ in (2.12), we obtain

$$(\mathbf{f},\mathbf{e}_i) - \mathcal{B}_h\big((\mathbf{u}_h,p_h),(\mathbf{e}_i,\epsilon_i)\big) \le j(\mathbf{u}_{i\tau}) - j(\mathbf{u}_{h\tau}).$$

Similarly, taking $(\mathbf{v},q) = (\mathbf{u}_h,p_h-p)$ in (2.6) gives

$$-(\mathbf{f},e) + B\big((\mathbf{u},p),(\mathbf{e},\epsilon)\big) \le j(\mathbf{u}_{h\tau}) - j(\mathbf{u}_\tau).$$

Thus

$$\begin{aligned} I_1 &\le j(\mathbf{u}_{i\tau}) - j(\mathbf{u}_\tau) \\ &= \int_\Gamma g|\mathbf{u}_{i\tau} - \mathbf{u}_\tau|\,ds \\ &\le j(\mathbf{e}_{i\tau}) - j(\mathbf{e}_\tau). \end{aligned}$$

We next calculate I_2. By the definition of the bilinear form $B(\cdot,\cdot)$ and the Green's formula,

$$\begin{aligned} B\big((\mathbf{u}_h,p_h),(\mathbf{e}-\mathbf{e}_i,\epsilon-\epsilon_i)\big) = {} & \sum_{K\in\mathcal{T}_h}(-\mu\Delta\mathbf{u}_h + \nabla p_h, \mathbf{e}-\mathbf{e}_i) \\ & + \sum_{E\in\mathcal{E}_h}\langle J_E, \mathbf{e}-\mathbf{e}_i\rangle + \sum_{K\in\mathcal{T}_h}(\operatorname{div}\mathbf{u}_h, \epsilon-\epsilon_i). \end{aligned} \tag{4.2}$$

Then, we have

$$\begin{aligned} I_2 &= -(\mathbf{f},\mathbf{e}_i-\mathbf{e}) + B\big((\mathbf{u},p),(\mathbf{e}_i-\mathbf{e},\epsilon_i-\epsilon)\big) + G(p_h,\epsilon_i) \\ &= -(\mathbf{f},\mathbf{e}_i-\mathbf{e}) + B\big((\mathbf{u}_h,p_h),(\mathbf{e}_i-\mathbf{e},\epsilon_i-\epsilon)\big) \\ &\quad + G(p_h,\epsilon_i) + B\big((\mathbf{e},\epsilon),(\mathbf{e}_i-\mathbf{e},\epsilon_i-\epsilon)\big) \\ &= \sum_{K\in\mathcal{T}_h}(\mathbf{R}_K,\mathbf{e}-\mathbf{e}_i) - \sum_{E\in\mathcal{E}_h}\langle J_E,\mathbf{e}-\mathbf{e}_i\rangle - \sum_{K\in\mathcal{T}_h}(\operatorname{div}\mathbf{u}_h,\epsilon_i-\epsilon) \\ &\quad + G(p_h,\epsilon_i) + B\big((\mathbf{e},\epsilon),(\mathbf{e}_i-\mathbf{e},\epsilon_i-\epsilon)\big). \end{aligned}$$

Noticing (2.14), we obtain

$$I_2 + B\big((\mathbf{e},\epsilon),(\mathbf{e}-\mathbf{e}_i,\epsilon-\epsilon_i)\big) = \sum_{K\in\mathcal{T}_h}(\mathbf{R}_K,\mathbf{e}-\mathbf{e}_i) - \sum_{E\in\mathcal{E}_h}\langle J_E,\mathbf{e}-\mathbf{e}_i\rangle - \sum_{K\in\mathcal{T}_h}(\operatorname{div}\mathbf{u}_h,\epsilon).$$

Therefore,

$$\begin{aligned} B\big((\mathbf{e},\epsilon),(\mathbf{e},\epsilon)\big) &= B\big((\mathbf{e},\epsilon),(\mathbf{e}_i,\epsilon_i)\big) + B\big((\mathbf{e},\epsilon),(\mathbf{e}-\mathbf{e}_i,\epsilon-\epsilon_i)\big) \\ &= I_1 + I_2 + B\big((\mathbf{e},\epsilon),(\mathbf{e}-\mathbf{e}_i,\epsilon-\epsilon_i)\big) \\ &\le j(\mathbf{e}_{i\tau}) - j(\mathbf{e}_\tau) + \sum_{K\in\mathcal{T}_h}(\mathbf{R}_K,\mathbf{e}-\mathbf{e}_i) \\ &\quad + \sum_{E\in\mathcal{E}_h}\langle J_E,\mathbf{e}-\mathbf{e}_i\rangle - \sum_{K\in\mathcal{T}_h}(\operatorname{div}\mathbf{u}_h,\epsilon). \end{aligned}$$

Due to the trace inequality and by straightforward calculation,

$$\begin{aligned} j(\mathbf{e}_{i\tau}) - j(\mathbf{e}_\tau) &\le \sum_{E\in\Gamma\cap\partial K}\|g\|_{\infty,E}\int_E|\mathbf{e}_\tau-\mathbf{e}_{i\tau}|\,ds \\ &\le \sum_{E\in\Gamma\cap\partial K}h_E^{1/2}\|g\|_{\infty,E}\|\mathbf{e}_\tau-\mathbf{e}_{i\tau}\|_{0,E} \\ &\le \sum_{E\in\Gamma\cap\partial K}h_E\|g\|_{\infty,E}\|\nabla\mathbf{e}\|_{0,K} \\ &\le \Bigg(\sum_{E\in\Gamma\cap\partial K}h_E^2\|g\|_{\infty,E}^2\Bigg)^{1/2}\|\nabla\mathbf{e}\|_0. \end{aligned}$$

Using the Cauchy–Schwarz inequality and the property of the Scott–Zhang interpolation, we obtain

$$\mu\|\nabla e\|_0^2 = B\big((\mathbf{e},\epsilon);(\mathbf{e},\epsilon)\big) \lesssim \eta\,|||(\mathbf{e},\epsilon)|||. \tag{4.3}$$

By the same approach as for Theorem 3.1, we next estimate $\|\epsilon\|_0$. Let $\mathbf{w}_h\in\bar{\mathbf{V}}_h$ be arbitrary and take $\mathbf{v}=\mathbf{u}\pm\mathbf{w}_h$ separately in (2.6) to obtain

$$a(\mathbf{u},\mathbf{w}_h) - d(\mathbf{w}_h,p) = (\mathbf{f},\mathbf{w}_h).$$

Also, taking $\mathbf{v}=\mathbf{u}_h\pm\mathbf{w}_h$ separately in (2.12), we have

$$a(\mathbf{u}_h,\mathbf{w}_h) - d(\mathbf{w}_h,p_h) = (\mathbf{f},\mathbf{w}_h).$$

Then, for all $\mathbf{w}_h\in\bar{\mathbf{V}}_h$, we have

$$a(\mathbf{e},\mathbf{w}_h) - d(\mathbf{w}_h,\epsilon) = 0. \tag{4.4}$$

Since $\epsilon \in Q$, there exists $\mathbf{w} \in [H_0^1(\Omega)]^2$ such that

$$d(\mathbf{w}, \epsilon) = \|\epsilon\|_0^2, \qquad \|\nabla \mathbf{w}\|_0 \lesssim \|\epsilon\|_0, \tag{4.5}$$

where the hidden constant is only dependent of Ω. Thus, by (4.4), for all $\mathbf{w}_h \in \bar{\mathbf{V}}_h$,

$$\begin{aligned} \|\epsilon\|_0^2 &= d(\mathbf{w}_h, \epsilon) + d(\mathbf{w} - \mathbf{w}_h, \epsilon) \\ &= a(\mathbf{e}, \mathbf{w}) + a(\mathbf{e}, \mathbf{w}_h - \mathbf{w}) + d(\mathbf{w} - \mathbf{w}_h, \epsilon). \end{aligned} \tag{4.6}$$

A straightforward calculation yields

$$a(\mathbf{e}, \mathbf{w}_h - \mathbf{w}) + d(\mathbf{w} - \mathbf{w}_h, \epsilon) = \sum_{K \in \mathcal{T}_h} (R_K, \mathbf{w} - \mathbf{w}_h) + \sum_{E \in \mathcal{E}_h} \langle J_E, \mathbf{w} - \mathbf{w}_h \rangle. \tag{4.7}$$

Now we choose $\mathbf{w}_h \in \bar{\mathbf{V}}_h$ such that

$$\|\mathbf{w} - \mathbf{w}_h\|_0 \leq C \|\nabla \mathbf{w}\|_0.$$

Therefore, using (4.5), (4.6) and (4.7), we deduce

$$\|\epsilon\|_0 \leq C\big(\|\nabla \mathbf{e}\|_0 + \eta\big). \tag{4.8}$$

Combining (4.3) and (4.8), we obtain (4.1). □

4.2 Efficiency

We notice that our reliable estimator derived in the previous section includes several terms. Among them, the terms $\|h_K R_K\|_{0,K}$, $\|\operatorname{div} \mathbf{u}_h\|_{0,K}$ and $\|h_E^{1/2} J_E\|_{0,E}$ appear even for Stokes problem with pure Dirichlet boundary conditions. By a standard argument (cf., [46, 47]), we can prove that the following efficiency results in conjecture 4.2 are also valid for Dirichlet boundary problems. The novelty in our estimator is that we have the new term $\|h_E^{\frac{1}{2}} g\|_{0,E}$ which comes from the slip boundary condition. In fact, the presented methods are still open on the efficiency in theory although numerical experiments reported in Sect. 5 is reliable and efficient. We have not been able to prove this fact yet.

Conjecture 4.2 *Let* $(\mathbf{u}, p)$ *and* $(\mathbf{u}_h, p_h)$ *be the solutions of* (2.6) *and* (2.12), *respectively. For each* $K \in \mathcal{T}_h$,

$$\|h_K R_K\|_{0,K} \lesssim \big|\!\big|\!\big|(\mathbf{u} - \mathbf{u}_h, p - p_h)\big|\!\big|\!\big|_K + \big\|h_K (R_K - \bar{R}_K)\big\|_{0,K}, \tag{4.9}$$

$$\|\operatorname{div} \mathbf{u}_h\|_{0,K} \lesssim \big|\!\big|\!\big|(\mathbf{u} - \mathbf{u}_h, p - p_h)\big|\!\big|\!\big|_K. \tag{4.10}$$

For each $E \in \mathcal{E}_h$,

$$\big\|h_E^{1/2} J_E\big\|_{0,E} \lesssim \big|\!\big|\!\big|(\mathbf{u} - \mathbf{u}_h, p - p_h)\big|\!\big|\!\big|_{\omega_E} + \sum_{K \subset \omega_E} \operatorname{osc}_K, \tag{4.11}$$

where the oscillation is defined for all $K \in \mathcal{T}_h$ *by*

$$\operatorname{osc}_K^2 = \left\| h_K(R_K - \bar{R}_K) \right\|_{0,K}^2 + \sum_{E \in \mathcal{E}_h \cap \partial K} h_E^{1/2} \|J_E - \bar{J}_E\|_{0,E}^2 + \sum_{E \in \Gamma \cap \partial K} \left\| h_E^{\frac{1}{2}}(g - \bar{g}_E) \right\|_{0,E}^2,$$

with $\bar{R}_K = \frac{1}{|K|}\int_K R_K$, $\bar{J}_E = \frac{1}{|E|}\int_E J_E$ *and* $\bar{g}_E = \frac{1}{|E|}\int_E g$ *denote the averages of* R_K *on* K, J_E *and* g *on* E, *respectively.*

5 Numerical experiments

In this section, we verify the theoretical findings in previous sections by the following three numerical examples: the first one is for a problem with a known smooth solution, the second one is for a problem on L-shape domain with a singular source $\mathbf{f}$, the final one is for the well-known driven cavity problem. All experiments are implemented by using the public free finite element software FreeFem++ [15]. Moreover, for a given mesh $\mathcal{T}_h$, the stabilized finite element system (2.12) is solved with Uzawa iteration by the lowest order pair $\mathbf{P}_1 - P_0$ and the lowest equal-order pair $\mathbf{P}_1 - P_1$, respectively.

In the sequel, we always use Dof to denote the cardinality of the triangulation $\mathcal{T}_h$. Let $\eta_g = (\sum_{E \in \Gamma \cap \partial K} h_E^2 \|g\|_{\infty,E}^2)^{1/2}$. Moreover, let $E_\eta = \frac{\eta}{|||(\mathbf{e},\epsilon)|||}$ be the effective index of our error estimator η.

5.1 A smooth problem

We consider (2.1) to (2.3) on the square $\Omega = [0,1]^2$ with $\mu = 1$, and

$$\mathbf{f} = \begin{pmatrix} 6x^2 - 6x^3 + y(3y-2)(6x-2) + 4y - 2 \\ 6y^3 - 6y^2 - x(3x-2)(6y-2) + 4x - 2 \end{pmatrix}.$$

The boundary of Ω is split into $\partial\Omega = \Gamma_D \cup \Gamma_1 \cup \Gamma_2$, where the Dirichlet boundary $\Gamma_D = (\{0\} \times [0,1]) \cup ([0,1] \times \{0\})$, the slip boundary $\Gamma = \Gamma_1 \cup \Gamma_2$ with $\Gamma_1 = \{1\} \times [0,1]$ and $\Gamma_2 = [0,1] \times \{1\}$. On Γ,

$$g(x,y) = \begin{cases} 4y^2(1-y), & (x,y) \in \Gamma_1, \\ 4x^2(1-x), & (x,y) \in \Gamma_2. \end{cases}$$

This problem admits a smooth solution

$$\mathbf{u} = \begin{pmatrix} -x^2 y(x-1)(3y-2) \\ xy^2(y-1)(3x-2) \end{pmatrix}, \qquad p = (2x-1)(2y-1).$$

Let $\mathcal{T}_1$ be an initial mesh obtained by partitioning the unit square into 10×10 equal squares and then dividing each square by connecting its diagonal into two triangles. Moreover, we let $\mathcal{T}_n$, $n = 2, \ldots, 7$ be a sequence of nested meshes satisfying $\#\mathcal{T}_n \simeq \#\mathcal{T}_{n-1}$, $n = 2, \ldots, 7$. We list the errors $|||(\mathbf{e},\epsilon)|||$, the special error estimator η_g, the error estimator η and the effectivity index E_η corresponding to these 7 meshes in Tables 1 and 2. From these

Table 1 Errors, estimators and effectivity ratio: $\mathbf{P}_1 - P_0$

Meshes	Dof	$\|\nabla \mathbf{e}\|_0$	$\|\epsilon\|_0$	$\|\|\|(\mathbf{e},\epsilon)\|\|\|$	η	η_g	E_η
$\mathcal{T}_1$	200	0.0781549	0.0827345	0.113812	0.48791	0.0836507	4.2870
$\mathcal{T}_2$	392	0.0555608	0.0583028	0.0805371	0.360565	0.0598029	4.4770
$\mathcal{T}_3$	800	0.0387081	0.0399877	0.0556537	0.257753	0.0418828	4.6314
$\mathcal{T}_4$	1800	0.0257007	0.0260654	0.036605	0.174117	0.0279351	4.7566
$\mathcal{T}_5$	3698	0.0178858	0.0178874	0.0252955	0.12227	0.0194876	4.8337
$\mathcal{T}_6$	7200	0.0127973	0.0126668	0.0180061	0.0879465	0.0139675	4.8843
$\mathcal{T}_7$	14,450	0.00902263	0.00885705	0.0126434	0.062228	0.00985919	4.9218

Table 2 Errors, estimators and effectivity ratio: $\mathbf{P}_1 - P_1$

Meshes	Dof	$\|\nabla \mathbf{e}\|_0$	$\|\epsilon\|_0$	$\|\|\|(\mathbf{e},\epsilon)\|\|\|$	η	η_g	E_η
$\mathcal{T}_1$	200	0.0775394	0.0357616	0.0853888	0.475923	0.0836507	5.5736
$\mathcal{T}_2$	392	0.0554011	0.0212961	0.0593532	0.342517	0.0598029	5.7708
$\mathcal{T}_3$	800	0.0387005	0.0122152	0.0405825	0.24037	0.0418828	5.9230
$\mathcal{T}_4$	1800	0.0257246	0.00648786	0.0265301	0.160261	0.0279351	6.0407
$\mathcal{T}_5$	3698	0.0179059	0.00370698	0.0182856	0.111726	0.0194876	6.1101
$\mathcal{T}_6$	7200	0.0128105	0.00221413	0.0130004	0.080006	0.0139675	6.1541
$\mathcal{T}_7$	14,450	0.00903022	0.00129542	0.00912266	0.0564323	0.00985919	6.1859

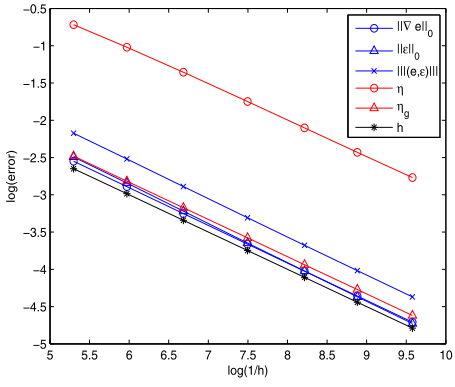

Figure 1 The convergence order on uniform-type mesh: $\mathbf{P}_1 - P_0$

tables, we find that the effectivity indices almost equal 5.0 and 6.0, respectively. These results imply that our error estimator is reliable and efficient for these examples. And this fact supports our analysis in Sect. 4.

In order to present precisely the convergence order of the errors, we plot the errors $\|\nabla \mathbf{e}\|_0$, $\|\epsilon\|_0$, $|||(\mathbf{e},\epsilon)|||$, the especial estimator η_g and the estimator η in Figs. 1 and 2. From the figures, we clearly observe that the errors $\|\nabla \mathbf{e}\|_0$, $\|\epsilon\|_0$, and $|||(\mathbf{e},\epsilon)|||$ converge to 0 with the order 1. This fact nicely support our theoretic result in Theorem 3.1. The convergence order of the pressure $\|\epsilon\|_0$ is between 1 and 2 in Fig. 2. This phenomenon may be surprising because we have used P_1 finite elements to approximate the pressure. Since the estimators η_g and η decrease also with the order 1, the analysis in Sect. 4 is also validated.

5.2 A problem on L-shape domain

We consider (2.1) to (2.3) on an L-shape domain $\Omega = [-1,1]^2 \setminus [0,1]^2$. Let the resource function

$$\mathbf{f} = \begin{pmatrix} -6r^{-0.5}\cos(0.5\theta) \\ -6r^{-0.5}\sin(0.5\theta) \end{pmatrix},$$

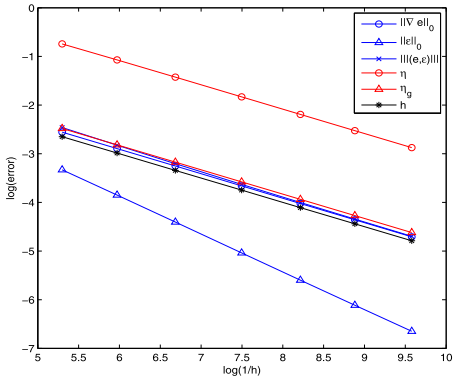

Figure 2 The convergence order on uniform-type mesh: $\mathbf{P}_1 - P_1$

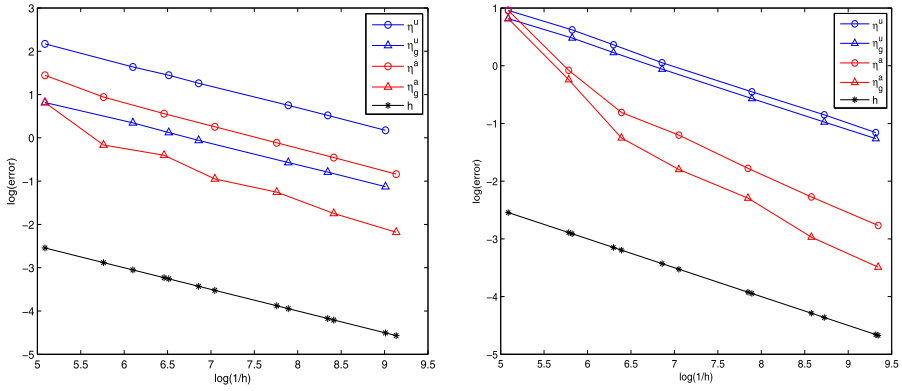

Figure 3 The convergence rate of adaptive and uniform refinements for the problem on L-shape domain with slip boundary condition: g is continuous at $(0,0)$. (**a**): $\mathbf{P}_1 - P_0$; (**b**): $\mathbf{P}_1 - P_1$

where (r,θ) is a polar representation of a point on the L-shape domain. Apparently $\mathbf{f}$ is singular at the corner of domain. The boundary $\partial\Omega$ is split into the Dirichlet boundary $\Gamma_D = ([-1,1]\times\{-1\})\cup(\{1\}\times[-1,0])\cup([-1,0]\times\{1\})\cup(\{-1\}\times[-1,1])$ and slip boundary $\Gamma = \partial\Omega\setminus\Gamma_D$.

Unlike the first example, the exact solution of this problem is not known. In this example, some singularities arise at the L-corner due to the singular source and the slip boundary conditions. We consider two choices for the scale function g. In the first example, g is, respectively, set as Sect. 5.1. In the second example,

$$g(x,y) = \begin{cases} 1, & (x,y)\in\Gamma_1, \\ 0.5, & (x,y)\in\Gamma_2, \end{cases}$$

where $\Gamma = \Gamma_1\cup\Gamma_2$ with $\Gamma_1 = [0,1]\times\{0\}$ and $\Gamma_2 = \{0\}\times[0,1]$. Obviously, g is discontinuous at point $(0,0)$ for the latter choice.

Observed from Figs. 3 and 4, the convergence results based on the a posteriori error estimates are shown. The adaptive refinement clearly leads to the optimal convergence rate of $O(h)$ approximated by the lowest finite element pair and equal-order finite element pair

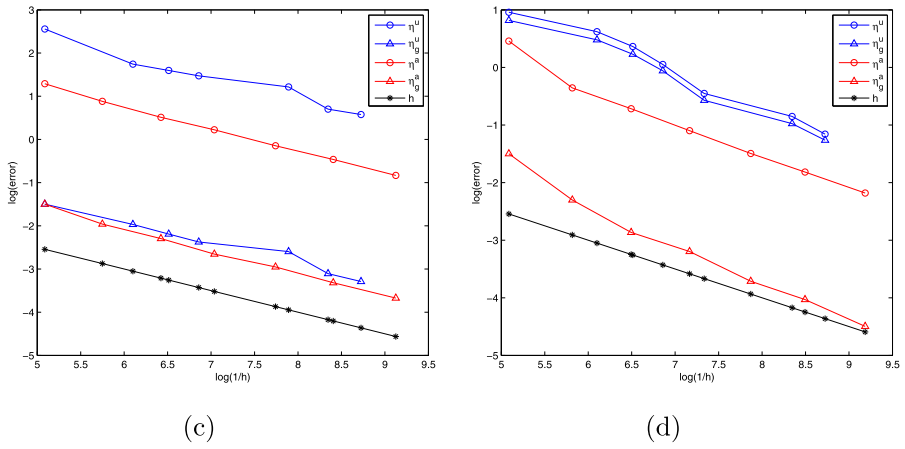

Figure 4 The convergence rate of adaptive and uniform refinements for the problem on L-shape domain with slip boundary condition: g is discontinuous at $(0,0)$. (**c**): $\mathbf{P}_1 - P_0$; (**d**): $\mathbf{P}_1 - P_1$

for the two different g. We note that the adaptive and uniform approaches can both leads to the optimal order rate of $O(h)$ if g is continuous at $(0,0)$. However, lots of unknowns are saved by the adaptive refinement to obtain the same accuracy. In the second example, the prominent advantage appears that the adaptive stabilized finite element methods have achieved the same convergence result as theoretical expectation for that lack of convexity of domains, but the convergence rate of the uniform refinement is reduced.

5.3 Lid driven cavity

Cavity flows have been widely used as test cases for validating the incompressible fluid dynamics algorithm. It is a popular benchmark problem for testing numerical schemes. In the classical test, the upper corners where the moving surface meets the stationary walls are singular points of the flow at which the horizontal velocity is multi-valued. Moreover, the lower corners are also weakly singular points. The fluid is enclosed in a square box with an imposed velocity of unity in the horizontal direction on the top boundary, and a no slip condition on the remaining walls. In our test, we impose a slip boundary condition to the bottom boundary, in fact, we let $u_2 = 0$, and set $g = 1.0, 10.0, 100.0$ and $\mu = 1.0$. We are thus able to study how meshes adapt to various effects on singularities by changing the slip boundary conditions.

Figures 5–10 show the adaptive refinements by the $\mathbf{P}_1 - P_0$ and $\mathbf{P}_1 - P_1$ stabilized methods, with different g. From Figs. 5–10, the choice of g has important effect on mesh distribution for the presented model since g is a major factor in the estimator, which is different from the Stokes equations with the Dirichlet boundary condition. Both singularities at upper and bottom definitely have important impact on the model presented here but the degree of impaction may be different. As observed from Fig. 5 with smallest $g = 1.0$, adaptive refinement is only generated in the two upper corners of the cavity. The affection of the slip boundary condition seems weak, only the influence of two singularities arising at the top corners of the square box are obviously found. As seen from Fig. 6 with $g = 10.0$, the influence of two singularities also increases at the two bottom corners, but it is a little weaker than that of the upper two singularities. As for Fig. 7 with $g = 100.0$, the influence of the singularities derived from the slip boundary condition increases and becomes a dom-

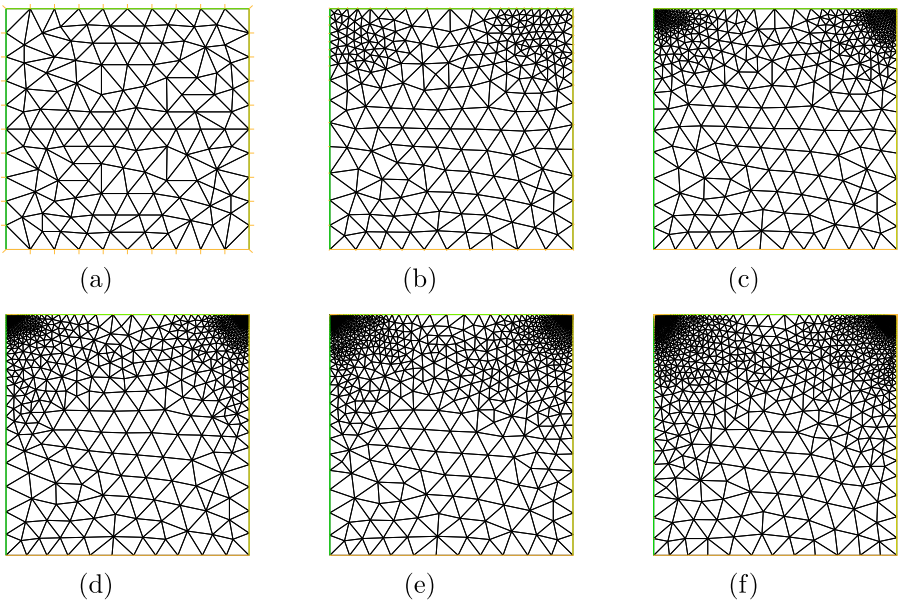

Figure 5 Adaptive refinements by $\mathbf{P}_1 - P_0$ stabilized method for the cavity flow with slip boundary condition: $g = 1.0$. (**a**): $\mathcal{T}_1$; (**b**): $\mathcal{T}_2$; (**c**): $\mathcal{T}_3$; (**d**): $\mathcal{T}_4$; (**e**): $\mathcal{T}_5$; (**f**): $\mathcal{T}_6$

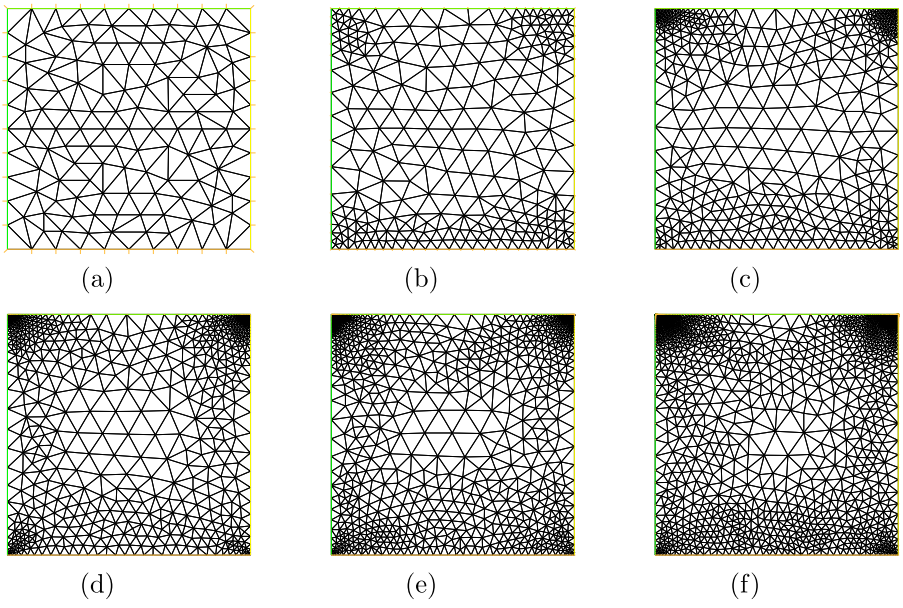

Figure 6 Adaptive refinements by $\mathbf{P}_1 - P_0$ stabilized method for the cavity flow with slip boundary condition: $g = 10.0$. (**a**): $\mathcal{T}_1$; (**b**): $\mathcal{T}_2$; (**c**): $\mathcal{T}_3$; (**d**): $\mathcal{T}_4$; (**e**): $\mathcal{T}_5$; (**f**): $\mathcal{T}_6$

inative factor as the given scalar function g increases. The adaptive refinements for the two stabilized methods are similar, which means both stabilized methods with adaptive strategy are effective to solve the incompressible flow with the slip boundary conditions of friction type.

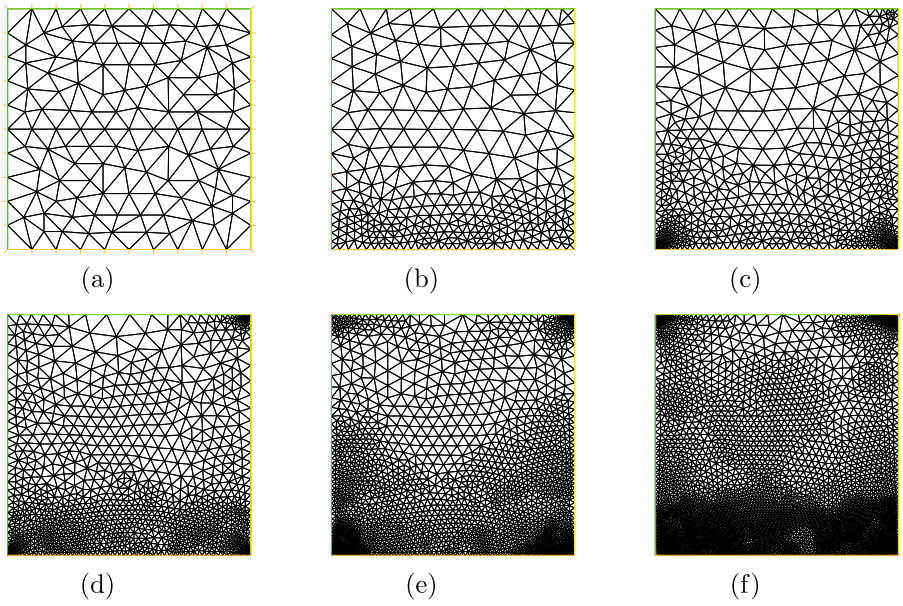

Figure 7 Adaptive refinements by $\mathbf{P}_1 - P_0$ stabilized method for the cavity flow with slip boundary condition: $g = 100.0$. (**a**): $\mathcal{T}_1$; (**b**): $\mathcal{T}_2$; (**c**): $\mathcal{T}_3$; (**d**): $\mathcal{T}_4$; (**e**): $\mathcal{T}_5$; (**f**): $\mathcal{T}_6$

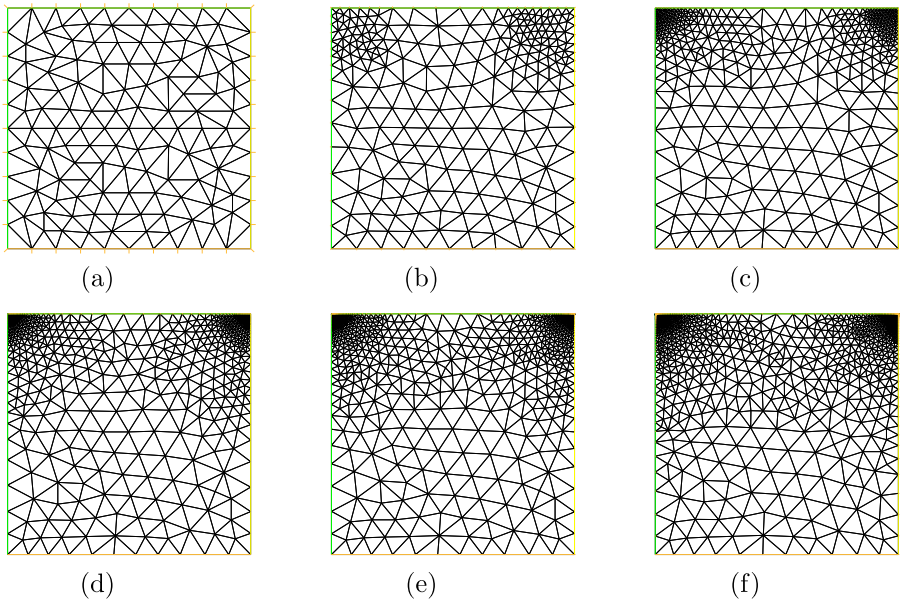

Figure 8 Adaptive refinements by $\mathbf{P}_1 - P_1$ stabilized method for the cavity flow with slip boundary condition: $g = 1.0$. (**a**): $\mathcal{T}_1$; (**b**): $\mathcal{T}_2$; (**c**): $\mathcal{T}_3$; (**d**): $\mathcal{T}_4$; (**e**): $\mathcal{T}_5$; (**f**): $\mathcal{T}_6$

6 Conclusion

In this paper, we consider the lower order stabilized finite element methods for the incompressible flow arising in arteriosclerosis. The velocity in H^1-norm and the pressure in L^2-norm decrease with optimal convergence orde. The reliable and efficient a posteriori error estimates for our finite element solutions are also derived. Moreover, we achieve a

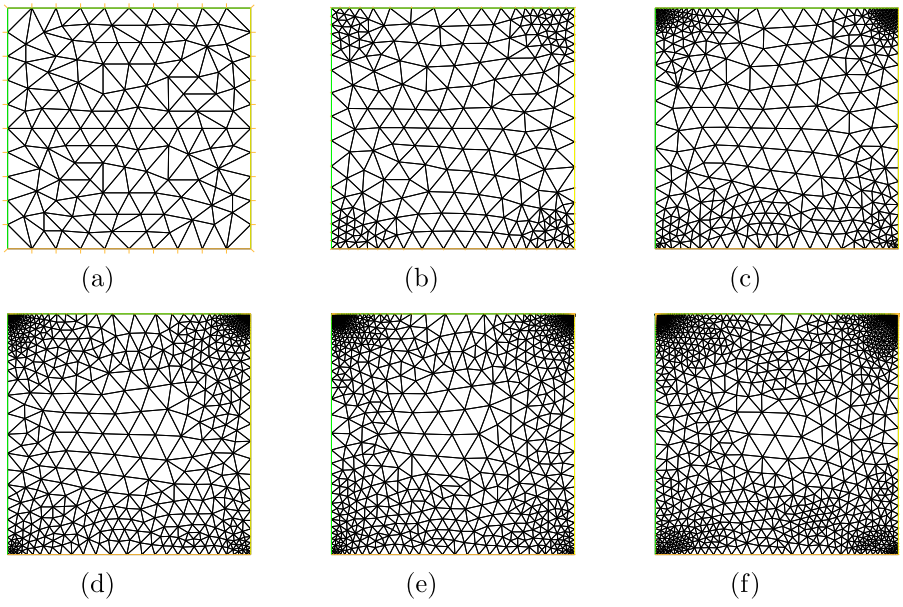

Figure 9 Adaptive refinements by $\mathbf{P}_1 - P_1$ stabilized method for the cavity flow with slip boundary condition: $g = 10.0$. (**a**): $\mathcal{T}_1$; (**b**): $\mathcal{T}_2$; (**c**): $\mathcal{T}_3$; (**d**): $\mathcal{T}_4$; (**e**): $\mathcal{T}_5$; (**f**): $\mathcal{T}_6$

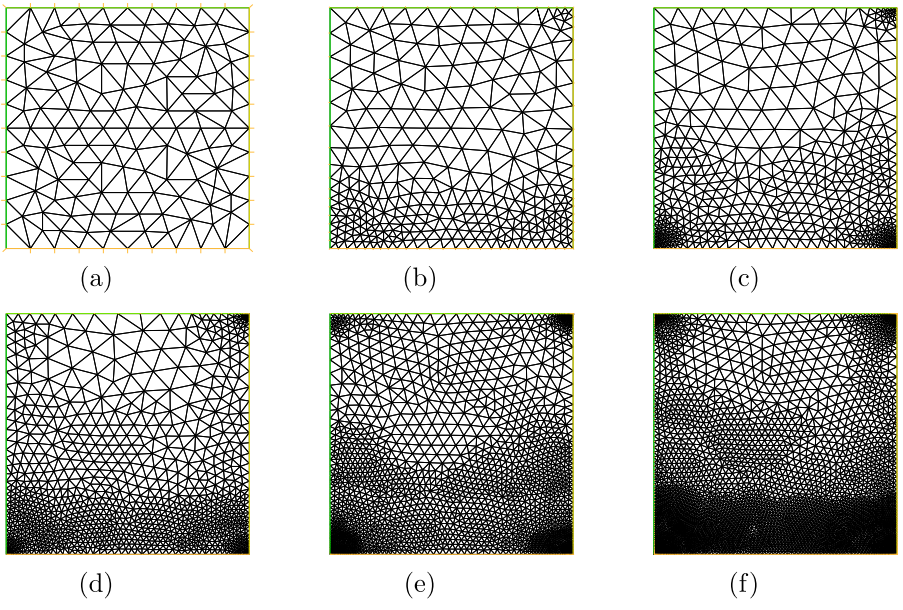

Figure 10 Adaptive refinements by $\mathbf{P}_1 - P_1$ stabilized method for the cavity flow with slip boundary condition: $g = 100.0$. (**a**): $\mathcal{T}_1$; (**b**): $\mathcal{T}_2$; (**c**): $\mathcal{T}_3$; (**d**): $\mathcal{T}_4$; (**e**): $\mathcal{T}_5$; (**f**): $\mathcal{T}_6$

series of numerical results for the presented problem [21–23]. Furthermore, we will then use the efficient methods [18, 34, 35, 37] to solve the similar practical problem for the coupling problem.

Acknowledgements
The authors would like to thank the editor and reviewers for the constructive comments and useful suggestions, which improved the manuscript.

Funding
The authors acknowledge financial supported in part by NSF of China (Grant Nos. 11771259, 11571384, and 11971174), special support program to develop innovative talents in the region of Shaanxi province, NSF of Shanghai (Grant No. 19ZR1414300), Science and Technology Commission of Shanghai Municipality (Grant No. 18dz2271000), the special project high performance computing of National Key Research and Development Program 2016YFB0200604, and by Guangdong Natural Science Foundation through grant 2017B030311001.

Availability of data and materials
Not applicable.

Competing interests
The authors declare that they have no competing interests.

Authors' contributions
All authors contributed equally to the manuscript and read and approved the final manuscript.

Author details
[1]Department of Mathematics, School of Arts and Sciences, Shaanxi University of Science and Technology, Xian, P.R. China. [2]School of Mathematical Sciences, Shanghai Key Laboratory of Pure Mathematics and Mathematical Practice, East China Normal University, Shanghai, P.R. China. [3]School of Data and Computational Science and Guangdong Province Key Laboratory of Computational Science, Sun Yat-sen University, Guangzhou, China.

Publisher's Note

Received: 12 February 2019 Accepted: 23 August 2019 Published online: 02 September 2019

References

1. Adams, R.A.: Sobolev Spaces. Academic Press, New York (1975)
2. Ainsworth, M., Oden, J.T.: A posteriori error estimators for the Stokes and Oseen equations. SIAM J. Numer. Anal. **34**, 228–245 (1997)
3. Arnold, D.N., Brezzi, F., Fortin, M.: A stable finite element for the Stokes equations. Calcolo **21**, 337–344 (1984)
4. Ayadi, M., Baffico, L., Goudra, M.K., Sassi, T.: Error estimates for Stokes problem with Tresca friction condition. ESAIM: M2AN **48**, 1413–1429 (2014)
5. Bank, R.E., Welfert, B.D.: A posteriori error estimates for the Stokes problem. SIAM J. Numer. Anal. **28**, 591–623 (1991)
6. Bayada, G., Boukrouche, M.: On a free boundary problem for the Reynolds equation derived from the Stokes system with Tresca boundary conditions. J. Math. Anal. Appl. **282**, 212–231 (2003)
7. Becker, R., Braack, M.: A finite element pressure gradient stabilization for the Stokes equations based on local projections. Calcolo **38**, 173–199 (2001)
8. Bochev, P., Dohrmann, C.R., Gunzburger, M.D.: Stabilization of low-order mixed finite elements for the Stokes equations. SIAM J. Numer. Anal. **44**, 82–101 (2006)
9. Brezzi, F.: On the existence, uniqueness and approximation of saddle-point problems arising form Lagrange multipliers. RAIRO. Anal. Numér. **8**, 129–151 (1974)
10. Brezzi, F., Pitkäanta, J.: On the stabilization of finite element approximations of the Stokes equations. In: Proceedings on the Efficient Solutions of Elliptic Systems, Kiel, 1984. Notes on Numerical Fluid Mechanics, vol. 10, p. 11. Vieweg, Braunschweig (1984)
11. Burman, E.: Pressure projection stabilizations for Galerkin approximations of Stokes' and Darcy's problem. Numer. Methods Partial Differ. Equ. **24**, 127–143 (2008)
12. Chen, Z.: Finite Element Methods and Their Applications. Springer, Heidelberg (2005)
13. Ciarlet, P.G.: The Finite Element Method for Elliptic Problems. North-Holland, Amsterdam (1978)
14. Dohrmann, C.R., Bochev, P.: A stabilized finite element method for the Stokes problem based on polynomial pressure projections. Int. J. Numer. Methods Fluids **46**, 183–201 (2004)
15. FreeFem++, version 2.17.1. http://www.freefem.org/
16. Fujita, H.: A mathematical analysis of motions of viscous incompressible fluid under leak or slip boundary conditions. RIMS Kôkyûroku **888**, 199–216 (1994)
17. Girault, V., Raviart, P.A.: Finite Element Method for Navier–Stokes Equations: Theory and Algorithms. Springer, Berlin (1987)
18. He, X., Li, J., Lin, Y., Ming, J.: A domain decomposition method for the steady-state Navier–Stokes–Darcy model with Beavers–Joseph interface condition. SIAM J. Sci. Comput. **37**, 264–290 (2015)
19. He, Y., Li, J.: A stabilized finite element method based on local polynomial pressure projection for the stationary Navier–Stokes equation. Appl. Numer. Math. **58**, 1503–1514 (2008)
20. Heywood, J.G., Rannacher, R.: Finite-element approximations of the nonstationary Navier–Stokes problem. Part I: regularity of solutions and second-order spatial discretization. SIAM J. Numer. Anal. **19**, 275–311 (1982)
21. Jing, F., Li, J., Chen, Z.: Stabilized finite element methods for a blood flow model of arterosclerosis. Appl. Math. Lett. **31**, 1713–2208 (2015)
22. Jing, F., Li, J., Chen, Z.: Discontinuous Galerkin methods for the incompressible flow with nonlinear leak boundary conditions of friction type. Appl. Math. Lett. **73**, 113–119 (2017)

23. Jing, F., Li, J., Chen, Z., Zhang, Z.: Numerical analysis of a characteristic stabilized finite element method for the time-dependent Navier–Stokes equations with nonlinear slip boundary conditions. J. Comput. Appl. Math. **320**, 43–60 (2017)
24. Kashiwabara, T.: On a finite element approximation of the Stokes problem under leak or slip boundary conditions of friction type. Publ. RIMS, Kyoto Univ. **40**, 345–383 (2004)
25. Kashiwabara, T.: Finite element method for Stokes equations under leak boundary condition of friction type. SIAM J. Numer. Anal. **51**, 2448–2469 (2013)
26. Kay, D., Silvester, D.: A posteriori error estimation for stabilized mixed approximations of the Stokes equations. SIAM J. Sci. Comput. **21**, 1321–1336 (1999)
27. Le Roux, C., Tani, A.: Steady solutions of the Navier–Stokes equations with threshold slip boundary conditions. Math. Methods Appl. Sci. **30**, 595–624 (2007)
28. Li, J., Chen, Z.: A new stabilized finite volume method for the stationary Stokes equations. Adv. Comput. Math. **30**, 141–152 (2009)
29. Li, J., Chen, Z.: Optimal L^2, H^1 and L^∞ analysis of finite volume methods for the stationary Navier–Stokes equations with large data. Numer. Math. **126**, 75–101 (2014)
30. Li, J., Chen, Z., He, Y.: A stabilized multi-level method of non-singular finite volume solutions of the stationary 3D Navier–Stokes equations. Numer. Math. **122**, 279–304 (2012)
31. Li, J., Chen, Z., Zhang, T.: Adaptive stabilized mixed finite volume methods for the incompressible flow. Numer. Methods Partial Differ. Equ. **31**, 1424–1443 (2015)
32. Li, J., He, Y.: A new stabilized finite element method based on two local Gauss integration for the Stokes equations. J. Comput. Appl. Math. **214**, 58–65 (2008)
33. Li, J., He, Y., Chen, Z.: A new stabilized finite element method for the transient Navier–Stokes equations. Comput. Methods Appl. Mech. Eng. **197**, 22–35 (2007)
34. Li, J., Huang, P., Zhang, C., Guo, G.: A linear, decoupled fractional time-stepping method for the nonlinear fluid–fluid interaction. Numer. Methods Partial Differ. Equ. (2019). https://doi.org/10.1002/num.22382
35. Li, J., Jing, F., Chen, Z., Lin, X.: A priori and a posteriori estimates of stabilized mixed finite volume methods for the incompressible flow arising in arteriosclerosis. J. Comput. Appl. Math. **363**, 35–52 (2020)
36. Li, J., Wang, J., Ye, X.: Superconvergence by L^2-projections for stabilized finite element methods for the Stokes equations. Int. J. Numer. Anal. Model. **6**, 711–723 (2009)
37. Li, J., Yao, M., Mahbub, M., Zheng, H.: The efficient rotational pressure-correction schemes for the coupling Stokes/Darcy problem. Comput. Math. Appl. https://doi.org/10.1016/j.camwa.2019.06.033
38. Li, R., Li, J., Chen, Z., Gao, Y.: A stabilized finite element method based on two local Gauss integrations for a coupled Stokes–Darcy. J. Comput. Appl. Math. **292**, 92–104 (2009)
39. Li, Y., Li, K.: Pressure projection stabilized finite element method for Navier–Stokes equations with nonlinear slip boundary conditions. Computing **87**, 113–133 (2010)
40. Li, Y., Li, K.: Pressure projection stabilized finite element method for Stokes problem with nonlinear slip boundary conditions. J. Comput. Appl. Math. **235**, 3673–3685 (2011)
41. Saidi, F.: Non-Newtonian Stokes flow with frictional boundary conditions. Math. Model. Anal. **12**, 483–495 (2007)
42. Saito, N.: On the Stokes equation with the leak or slip boundary conditions of friction type: regularity of solutions. Publ. RIMS **40**, 345–383 (2004)
43. Scott, L.R., Zhang, S.: Finite element interpolation of nonsmooth functions satisfying boundary conditions. Math. Comput. **54**, 483–493 (1990)
44. Silvester, D.: Optimal low order finite element methods for incompressible flow. Comput. Methods Appl. Mech. Eng. **111**, 357–368 (1994)
45. Temam, R.: Navier–Stokes Equations. North-Holland, Amsterdam (1984)
46. Verfurth, R.: A posteriori error estimators for the Stokes equations. Numer. Math. **55**, 309–325 (1989)
47. Wang, J., Wang, Y., Ye, X.: A posteriori error estimate for stabilized finite element methods for the Stokes equations. Int. J. Numer. Anal. Model. **9**, 1–16 (2012)
48. Zheng, H., Hou, Y., Shi, F.: A posteriori error estimates of stabilization of low-order mixed finite elements for incompressible flow. SIAM J. Sci. Comput. **32**, 1346–1360 (2010)